JOURNAL OF GUIDANCE, CONTROL, AND DYNAMICS
Vol. 35, No. 3, May–June 2012

Time-Varying Dynamics of a Micro Air Vehicle with Variable-Sweep Morphing

Animesh Chakravarthy*
Wichita State University, Wichita, Kansas 67260
and
Daniel T. Grant† and Rick Lind‡
University of Florida, Gainesville, Florida 32611

DOI: 10.2514/1.55078

In this paper, the longitudinal dynamics of a fast-morphing, variable-wing-sweep micro air vehicle are investigated from a flight dynamics perspective. The time scales over which the morphing occurs are of the same order as the flight dynamics of the micro air vehicle, due to which the time-varying aspects of the dynamics must be carefully evaluated. The time-varying characteristic equation (which represents a generalization of the standard linear time-invariant characteristic equation) for this micro air vehicle is presented in analytic form, and this enables a characterization of the influence of different morphing trajectories on the flight dynamics. The concept of a time-varying pole is subsequently adopted and the flight dynamic properties of the time-varying modes are determined. A tool to properly evaluate the sensitivity of the time-varying modes to different morphing trajectories is demonstrated.

Nomenclature

$A_0(t), A_1(t), A_2(t), A_3(t)$	=	coefficients of time-varying characteristic equation
$E_i(t)$	=	energy associated with ith mode
F_x	=	derivative of generalized force F with respect to state x
g	=	acceleration due to gravity, m/s^2

Animesh Chakravarthy is an assistant professor with a joint appointment in the Departments of Aerospace Engineering and Electrical Engineering at Wichita State University. He obtained his Master's Degree in Aerospace Engineering at the Indian Institute of Science in 1994, and his Ph.D in the Department of Aeronautics and Astronautics at the Massachusetts Institute of Technology in 2007, with specialization in Estimation and Control. From 1994 to 2001 he was a Scientist/Engineer at the Aeronautical Development Agency, India in the Flight Mechanics and Control Division and from 2007 to 2010 he was a research scientist at the University of Florida Research and Engineering Education Facility. He has been on the faculty at Wichita State University since 2011. His research interests include dynamics and control of morphing vehicles, path planning in dynamic environments, multivehicle systems and study of insect flight dynamics.

Daniel T. Grant was born in Gainesville, FL in 1983. He received his B.S. degree with honors, his M.S. degree, and his Ph.D. in Aerospace Engineering from the University of Florida in 2006, 2008, and 2011, respectively. Since his graduation he has worked for a mining and construction company, where he currently holds the title of Controls and Automation Design Engineer and is heading research to develop fully autonomous mining equipment. His current interests include autonomous vehicle control, advanced algorithm design, and micro aerial vehicles research and development.

Rick Lind is an associate professor in the Department of Mechanical and Aerospace Engineering at the University of Florida. He received a B.S. in Astrophysics and a B.S. in Physics in 1990, a M.S. in Aerospace Engineering in 1993, and a Ph.D. in Aerospace Engineering in 1995 from the University of Minnesota. He was a research engineer for NASA at the Dryden Flight Research Center from 1996 until 2001 when he joined the faculty at the University of Florida. He is an Associate Fellow of AIAA and a member of the Structural Dynamics Technical Committee and the Atmospheric Flight Mechanics Technical Committee, along with being on the Editorial Board for the AIAA Progress in Aeronautics and Astronautics book series. Also, he will serve as the General Chair of the 2013 Atmospheric Flight Mechanics Conference. A primary focus of his research has been biologically inspired technologies for autonomous flight of aeroelastic vehicles.

Received 24 May 2011; revision received 5 September 2011; accepted for publication 5 September 2011.

*Assistant Professor, Department of Aerospace Engineering and Department of Electrical Engineering; animesh.chakravarthy@wichita.edu. Senior Member AIAA.
†Graduate Student, Department of Mechanical and Aerospace Engineering; dtgrant@ufl.edu. Student Member AIAA.
‡Associate Professor, Department of Mechanical and Aerospace Engineering; ricklind@ufl.edu. Associate Fellow AIAA.

M = pitching moment, N-m
$p_{4i}(t)$ = ith right pole of a fourth-order system
$p_R(t)$ = real part of right pole
$p_I(t)$ = imaginary part of right pole
$q(t)$ = pitch rate, rad/s
$s_{p4i}(t)$ = sensitivity of ith right pole of fourth-order system
$s_{\phi 4i}(t)$ = sensitivity of ith mode of fourth-order system
X = longitudinal force, N
$x(t)$ = state vector
$u(t)$ = longitudinal velocity (m/s)
$v_i(t)$ = ith eigenvector associated with a right pole
$w(t)$ = normal velocity, m/s
Z = normal force, N
$\theta(t)$ = pitch attitude, rad
$\mu(t)$ = morphing trajectory, rad
$\phi_{4i}(t)$ = ith mode of a fourth-order system
$\omega(t)$ = time-varying frequency

I. Introduction

MANY studies into morphing aircraft have focused on the steady-state benefits of altering a configuration for issues such as fuel consumption, range and endurance, cost and logistics, actuator energy, maneuverability and airfoil requirements [1–7]. There have also been studies with predominant focus on aerodynamic performance and materials, that have demonstrated clear benefits of morphing as measured by aerodynamic performance metrics [8]. Several aeroelastic effects of morphing have also been studied relative to maximum roll rate and actuator loads [9–12]. Morphing has been cast as a reinforcement learning problem [13], been analyzed for actuator power requirements [14], and also employed for maneuvers such as perching [15]. Other investigations have considered control of morphing systems [16]. A study using piezoelectric materials designed control only to achieve roll [17]. A variety of other studies that have investigated control have done so mostly in the context of actuation energy [18] and control authority [19] for simple changes in flight condition. Some studies have considered morphing for control surfaces [20,21] while others have used a morphing model with a distributed set of control effectors [22] rather than a shape with fully time-varying dynamics.

Time-varying dynamics have been noted on a variety of aerospace systems. These effects have been extensively studied on space systems for issues such as a translating mass within a space station [23], a moving mass on a solar-sail vehicle [24], a Coulomb tether that controls the mass distribution of a two-vehicle system [25], a moving flexible appendage [26], mass expenditure due to thrusters [27], and fluid sloshing [28]. The effects on rigid aircraft are not as prevalent due to the time scale of the dynamics relative to any mass changes; however, studies have noted the influence of rapid changes in mass during aerial refueling [29] and even motion due to flapping [30].

The introduction of morphing, or shape-changing actuation, to an aircraft will alter the shape and aerodynamics of the vehicle and so is a clear cause of time-varying effects. These time-varying effects can have a profound influence on system performance and must be considered for some applications. In this paper, an example of a variable-sweep micro air vehicle (MAV) [31] is used to indicate these influences. This double wing section MAV has the capability to independently vary the sweep of the inboard and outboard sections of each wing. The wings are able to sweep on the order of a second; and since this is of the same order of magnitude as the flight dynamics, the time-varying nature of the morphing must be considered, i.e., the MAV cannot be approximated as a piecewise linear time-invariant (LTI) system and standard tools of LTI analysis are not applicable for such a system. The time-varying nature of morphing is studied by analyzing the MAV as a linear time-varying (LTV) system; and examining the time-varying modes that ensue due to the occurrence of a disturbance that hits the MAV at the same time as it is morphing.

Several notions of poles and zeros of LTV systems have been discussed in the literature [32–35]. For an LTI system, use of the Laplace transform converts the system to an algebraic representation whose numerator and denominator can then be factorized in a conventional manner, to obtain the poles and zeros of the system. For an LTV system, however, use of the Laplace transform does not (in general) convert the system to an algebraic representation; therefore one notion [32] invokes the use of special factorization techniques that work directly on the ordinary differential equations (ODEs), to obtain the LTV poles and zeros. In another notion [35], the concept of extended eigenvalues and eigenvectors (or x-eigenvalues and x-eigenvectors) for LTV systems is introduced. This notion was further built upon [33] by demonstrating that performing a QR decomposition of the state transition matrix of the LTV system can lead to the computation of the LTV poles of that system. In [34], notions of Parallel D spectra and Series D spectra are used to characterize features of LTV system dynamics.

The contributions of this paper are as follows:

1) It presents an analytical representation of the LTV characteristic equation of the longitudinal dynamics of a variable-sweep morphing MAV in the form of an ODE with time-varying coefficients. These coefficients can also be written explicitly in terms of the morphing trajectory and this represents a generalization of the characteristic equation of LTI aircraft, to morphing LTV aircraft.

2) It discusses time-varying counterparts of the conventional short-period and phugoid modes, for fast morphing trajectories for which the MAV cannot be approximated as a piecewise LTI system.

3) It uses the LTV characteristic equation to introduce a concept that demonstrates the (continuous) sensitivity of the time-varying modes to different morphing trajectories.

II. Time-Varying Poles

A. Computation

1. *Two-State System*

A concept of poles for a LTV system is derived using a factorization approach [32] that is related to an argument using Parallel D Spectra and Series D Spectra [34]. This concept is derived for nth-order systems; however, the derivation for a second-order system is useful for tutorial purposes. Consider a LTV system Eq. (1) that is equivalently written using operator notation $D = \frac{\mathrm{d}}{\mathrm{d}t}$ as in Eq. (2)

$$0 = \ddot{y} + a_1(t)\dot{y} + a_0(t)y(t) \tag{1}$$

$$= (D^2 + a_1(t)D + a_0(t))y(t) \tag{2}$$

The above expression may be factorized if there exist functions, $p_1(t)$ and $p_2(t)$, as in Eq. (3) related by a noncommutative polynomial multiplication o, as in Eq. (4)

$$(D^2 + a_1(t)D + a_0(t))y(t) = (D - p_1(t))\{(D - p_2(t))y(t)\} \tag{3}$$

$$= \{(D - p_1(t))o(D - p_2(t))\}y(t) \tag{4}$$

An equation which determines $p_2(t)$ results from defining $Do p_2(t) = p_2(t)D + \dot{p}_2(t)$ as given in Eq. (5)

$$p_2^2(t) + \dot{p}_2(t) + a_1(t)p_2(t) + a_0(t) = 0 \tag{5}$$

A corresponding expression is also derived for $p_1(t)$ in Eq. (6)

$$p_1(t) + p_2(t) = -a_1(t) \tag{6}$$

The pair $(p_1(t), p_2(t))$ form a pole set with $p_2(t)$ being called a right pole. Note that this pair is an ordered pole set. These poles are unique up to the choice of the initial condition. With each time-varying right pole, there is an associated mode, which is given by $\phi_{p2}(t, 0) = e^{\int_0^t p_2(\tau)\,\mathrm{d}\tau}$. The system Eq. (1) actually has a pair of right poles and a pair of left poles. The pair of right poles results from solving Eq. (5) from a pair of different initial conditions on these poles. Such a pair of

initial conditions might be having $(p_{21}(0), p_{22}(0))$ relate to the poles from the time-invariant dynamics before morphing is started; however, there can be some conditions under which such a choice of initial values can lead to unbounded poles $p_{21}(t)$ and/or $p_{22}(t)$. For second-order LTV systems, a phase plane analysis has been used [36] to determine an analytical representation of these conditions; under which an alternative choice of initial values $(p_{21}(0), p_{22}(0))$ would have to be used. Either way, the right poles are sufficient to describe the system since the left poles are simply their counterparts as described by Eq. (6). Associated with each pole are also a set of eigenvectors. Each eigenvector v_i and its associated pole p_{2i} must satisfy Eq. (7)

$$(A(t) - p_{2i}(t))v_i(t) = \dot{v}_i(t) \tag{7}$$

where $A(t)$ is the system matrix, which for Eq. (1) has the structure

$$A(t) = \begin{bmatrix} 0 & 1 \\ -a_0(t) & -a_1(t) \end{bmatrix} \tag{8}$$

The state response $x(t)$ is finally written in Eq. (9) in terms of these time-varying parameters. Note that this response depends on modes, which relates to the integral of the poles, as opposed to depending directly on the poles

$$x(t) = C_1 v_1(t)\phi_{21}(t, 0) + C_2 v_2(t)\phi_{22}(t, 0) \tag{9}$$

where C_1 and C_2 depend not only the initial conditions on the states $x(0)$, but also on the initial conditions of the poles $(p_{21}(0), p_{22}(0))$.

2. *Four-State System*

The generalized form of a four-state system is expressed in Eq. (10). In this case, the derivatives of the state $w(t)$ are multiplied by real coefficients of $A_0(t)$, $A_1(t)$, $A_2(t)$, $A_3(t)$. The expression is altered using operator notation, given as $D = \frac{\mathrm{d}}{\mathrm{d}t}$ as in Eq. (2), to generate Eq. (11)

$$0 = \frac{\mathrm{d}^4 w}{\mathrm{d}t^4} + A_3(t)\frac{\mathrm{d}^3 w}{\mathrm{d}t^3} + A_2(t)\frac{\mathrm{d}^2 w}{\mathrm{d}t^2} + A_1(t)\frac{\mathrm{d}w}{\mathrm{d}t} + A_0(t)w \tag{10}$$

$$= (D^4 + A_3(t)D^3 + A_2(t)D^2 + A_1(t)D + A_0(t))w(t) \tag{11}$$

The concept of an ordered set of poles, $(p_1(t), p_2(t), p_3(t), p_4(t))$ is used, to relate to the dynamics as in Eq. (12)

$$\begin{aligned}(D^4 + A_3(t)D^3 + A_2(t)D^2 + A_1(t)D + A_0(t))w(t) \\ = (D - p_1(t))[(D - p_2(t)\{(D - p_3(t))[D - p_4(t)]\}]w\end{aligned} \tag{12}$$

The right pole, which is the only pole needed to fully characterize the response of the system is generated as a solution to Eq. (13). Note that again the right pole, $p_4(t)$, actually has four values of $p_{4i}(t)$ resulting from choice of initial conditions for the poles

$$\begin{aligned}0 = \frac{\mathrm{d}^3 p_{4i}}{\mathrm{d}t^3} + (4p_{4i}(t) + A_3(t))\frac{\mathrm{d}^2 p_{4i}}{\mathrm{d}t^2} + (6p_{4i}^2(t) + A_2(t) \\ + 3A_3(t)p_{4i}(t))\frac{\mathrm{d}p_{4i}}{\mathrm{d}t} + 3\left(\frac{\mathrm{d}p_{4i}}{\mathrm{d}t}\right)^2 + p_{4i}^4(t) + A_3(t)p_{4i}^3(t) \\ + A_2(t)p_{4i}^2(t) + A_1(t)p_{4i}(t) + A_0(t)\end{aligned} \tag{13}$$

A set of eigenvectors are again associated with each pole. Each eigenvector v_i and its associated pole p_{4i} must satisfy Eq. (14)

$$(A(t) - p_{4i}(t))v_i(t) = \dot{v}_i(t) \tag{14}$$

The states of the system are computed as a linear combination of these eigenvectors and the modes, given as $\phi_{4i} = \exp(\int_0^t p_{4i}(t))$, associated with each pole. The resulting expression is given along with the scalar constants C_i in Eq. (15)

$$\begin{aligned}x(t) = C_1 v_1(t)\phi_{41}(t) + C_2 v_2(t)\phi_{42}(t) + C_3 v_3(t)\phi_{43}(t) \\ + C_4 v_4(t)\phi_{44}(t)\end{aligned} \tag{15}$$

The decomposition of the states into the form of Eq. (15) indicates the time-varying parameters essentially diagonalize the system. In other words, a matrix defined as $V(t) = [v_1(t)|v_2(t)|v_3(t)|v_4(t)]$ will diagonalize the system matrix as long as $V(t)$ is invertible and bounded.

The stability of the system is determined by the relationship in Eq. (15). Essentially, the system has asymptotic stability for which states will tend to equilibrium if and only if the magnitude of the mode goes to zero as time increases. This condition, which is expressed as $|\phi_{4i}| \to 0$ as $t \to \infty$ for each $i = 1, 2, 3, 4$, is equivalent to a condition on the real part of the pole being $\int_0^\infty p_R(\tau)\,\mathrm{d}\tau < 0$.

B. Modal Interpretation

The concept of modal parameters is used in the dynamic community to disseminate the behavior of a system in terms of a few common characteristics. The parameters of natural frequency and damping are commonly used as such characterizations of LTI systems. The evaluation of LTV systems cannot immediately use these same definitions; however, related concepts of periodicity and decay envelope have essential similarity and are readily available.

Consider the oscillatory response of a two-state system, as originally given in Eq. (9), with the coefficients normalized to ease presentation as in Eq. (16). Also, assume the generalized poles to be complex conjugates such that $p_{21} = p_{22}^* = p_R + \jmath p_I$ as in Eq. (17). The complex exponentials can then be expressed in terms of sines and cosines as in Eq. (17)

$$\phi_{21}(t) = e^{\int_0^t p_{21}(\tau)\,\mathrm{d}\tau} = e^{\int_0^t (p_R(\tau) + \jmath p_I(\tau))\,\mathrm{d}\tau} \tag{16}$$

$$= e^{\int_0^t p_R(\tau)\,\mathrm{d}\tau}\cos\left(\int_0^t p_I(\tau)\,\mathrm{d}\tau\right) + \jmath e^{\int_0^t p_R(\tau)\,\mathrm{d}\tau}\sin\left(\int_0^t p_I(\tau)\,\mathrm{d}\tau\right) \tag{17}$$

An oscillatory response with decay is demonstrated in Eq. (17). The nature of the oscillations and the decay are both determined by the integrals of real and imaginary parts of these poles.

The decaying nature of the response, which is similar to the damping of a linear time-invariant system, is determined by the varying magnitude of the exponential in Eq. (17). The resulting envelope is given in Eq. (18) by adding the complex-conjugate poles

$$\text{envelope } (\phi(t)) = e^{\int_0^t p_R(\tau)\,\mathrm{d}\tau} = e^{\int_0^t \frac{p_{21}(\tau) + p_{22}(\tau)}{2}\,\mathrm{d}\tau} \tag{18}$$

The oscillations occur with a frequency related to the imaginary part of the time-varying pole. The time-varying natural frequency $\omega(t)$ is obtained from Eq. (17) and given in Eq. (19)

$$\omega(t) = \frac{\int_0^t p_I(\tau)\,\mathrm{d}\tau}{t} \tag{19}$$

C. Sensitivity

The preceding discussion assumed a particular trajectory for the time-variation of $A_3(t)$, $A_2(t)$, $A_1(t)$ and $A_0(t)$ in Eq. (11). For morphing aircraft, however, there can exist some control over the choice of these trajectories (details of this are given in subsequent sections). Using the notation $\mu(t)$ to represent a morphing trajectory, for a given morphing duration of $[0, t_f]$ with given values of $\mu(0)$ and $\mu(t_f)$, there can exist multiple morphing trajectories connecting these two configurations. Only one linear function exists to connect the two points $(\mu(0), 0)$ and $(\mu(t_f), t_f)$ in (μ, t) space whereas multiple quadratic functions exist to connect the same two points. The class of quadratic functions under consideration are given in Eq. (20) using real constants of a, b, and c

$$\mu(t) = \begin{cases} at^2 + bt + c & t <= t_f \\ at_f^2 + bt_f + c & t > t_f \end{cases} \tag{20}$$

which for fixed values of $\mu(0)$ and $\mu(t_f)$ takes the form

$$\mu(t) = \begin{cases} at^2 + (\mu(t_f) - \mu(0) - at_f^2)t/t_f + \mu(0) & t <= t_f \\ \mu(t_f) & t > t_f \end{cases} \tag{21}$$

To be able to analyze the relative effects of the multiple $\mu(t)$ trajectories possible with Eq. (20), we can generalize Eq. (12) to have the following form:

$$\begin{aligned}(D^4 + A_3(\mu(t))D^3 + A_2(\mu(t))D^2 + A_1(\mu(t))D \\ + A_0(\mu(t)))w(\mu(t)) = (D - p_1(\mu(t)))[(D - p_2(\mu(t)) \\ \{(D - p_3(\mu(t)))[D - p_4(\mu(t))]\}]w(\mu(t))\end{aligned} \tag{22}$$

Different morphing trajectories will lead to different dynamics and thus different modal behavior. It is important to relate the different modes with the different morphing trajectories. A measure of sensitivity to the morphing trajectory provides valuable information about the poles and modes. Such a measure indicates the amount by which the poles and modes, and consequently the response, will vary for a given change in the morphing trajectory. A sensitivity, $s_{p_{4i}}(t) \equiv \frac{\mathrm{d}p_{4i}}{\mathrm{d}\mu} = \frac{\mathrm{d}p_{4i}}{\mathrm{d}a}\frac{\mathrm{d}a}{\mathrm{d}\mu}$, is introduced in this paper and computed for each pole, $p_{4i}(t)$, associated with a fourth-order system using the relationship of Eq. (23). This relationship includes coefficients of A_0, A_1, A_2, A_3 from the original dynamics in Eq. (11), which are time-varying parameters due to dependency on the morphing

$$\begin{aligned}0 = {} & \frac{\mathrm{d}^3 s_{p_{4i}}}{\mathrm{d}t^3} + (4p_{4i} + A_3(\mu))\frac{\mathrm{d}^2 s_{p_{4i}}}{\mathrm{d}t^2} + (6p_{4i}^2 + A_2(\mu) \\ & + 3A_3(\mu)p_{4i})\frac{\mathrm{d}s_{p_{4i}}}{\mathrm{d}t} + \dot{p}_{4i}\left(12p_{4i}s_{p_{4i}} + \frac{\mathrm{d}A_2(\mu)}{\mathrm{d}\mu} + 3A_3(\mu)s_{p_{4i}}\right. \\ & \left. + 3\frac{\mathrm{d}A_3(\mu)}{\mathrm{d}\mu}p_{4i}\right) + 6\dot{p}_{4i}\frac{\mathrm{d}s_{p_{4i}}}{\mathrm{d}t} + 4p_{4i}^3 s_{p_{4i}} + \frac{\mathrm{d}A_2(\mu)}{\mathrm{d}\mu}p_{4i}^2 \\ & + 2A_2(\mu)p_{4i}s_{p_{4i}} + \frac{\mathrm{d}A_3(\mu)}{\mathrm{d}\mu}p_{4i}^3 + 3A_3(\mu)p_{4i}^2 s_{p_{4i}} \\ & + \frac{\mathrm{d}A_1(\mu)}{\mathrm{d}\mu}p_{4i} + A_1(\mu)s_{p_{4i}} + \frac{\mathrm{d}A_0(\mu)}{\mathrm{d}\mu}\end{aligned} \tag{23}$$

An expression for the sensitivity of the modes follows directly from the relationship $\phi_{4i} = \exp(\int_0^t p_{4i}(t))$. The resulting sensitivity, $s_{\phi_{4i}}(t)$, is given in Eq. (24)

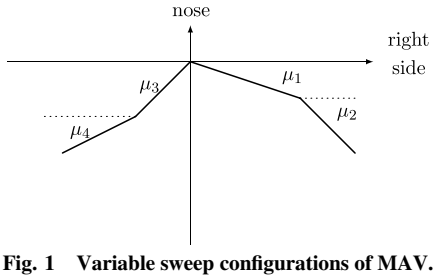

Fig. 1 Variable sweep configurations of MAV.

$$s_{\phi_{4i}}(t) = \phi_{4i}(t)\int_0^t s_{p_{4i}}(t)\,\mathrm{d}t \tag{24}$$

These sensitivities are useful indicators of the effect of variations in morphing rate when limiting the trajectories to the quadratic functions of Eq. (21). Essentially, these trajectories can be parameterized entirely by the coefficients so the sensitivity can also be parameterized entirely by the coefficients. Consider a morphing trajectory characterized by the coefficient set of $\{a, b, c\}$ and another morphing trajectory characterized by $\{a + \Delta a, b, c\}$. The time-varying modes will differ for these trajectories as in Eq. (25) where the mode and its sensitivity are noted as being computed with respect to the coefficients of the morphing trajectory

$$\phi_{4i}(t)|_{a+\Delta a} = \phi_{4i}(t)|_a + s_{\phi_{4i}}(t)_a \Delta a + \ldots\ldots \tag{25}$$

The evaluation of sensitivity can actually be considered at each instant in time or integrated across a span of time. The instantaneous sensitivity indicates how varied the mode may be at a given time instant while the integrated sensitivity indicates a cumulative variation in the mode.

The concept of mode sensitivity is also a useful tool in determining the properties of that specific morphing trajectory that will lead to good disturbance rejection properties of a mode. This is seen as follows. The energy E_i of the ith mode is given by $E_i = \int_0^\infty \phi_{4i}(t)^2\,\mathrm{d}t$. From the class of morphing trajectories defined in Eq. (20), the one that corresponds to an energy extremum will satisfy $\frac{\mathrm{d}E_i}{\mathrm{d}a} = 0 \Rightarrow \int_0^\infty \phi_{4i}(t)s_{\phi_{4i}}(t)\,\mathrm{d}t = 0$. In other words, this particular morphing trajectory will correspond to those value(s) of a such that the mode and its sensitivity are orthogonal functions. For these specific value(s) of a, further checking if $\frac{\mathrm{d}^2 E_i}{\mathrm{d}a^2} < 0$ enables the determination of whether that extremum corresponds to a minima; which in turn means that the morphing trajectory corresponding to that value of a has good disturbance rejection properties.

III. Aircraft

A. Design

A vehicle is designed to admit variations in the sweep angle of each wing. Figure 1 is a schematic representation of the possible degrees of freedom in the sweep angle variation. The basic construction uses skeletal members of a prepregnated, bidirectional carbon fiber weave along with rip-stop nylon. The fuselage and wings are entirely constructed of the weave while the tail features carbon spars covered with nylon. The resulting vehicle has a weight of 596 g and a fuselage length of 48 cm.

The wings actually consist of separate sections which are connected to the fuselage and each other through a system of spars and joints. These joints are representative of an elbow and a wrist which serve to vary the sweep of inboard and outboard wing sections. The range of horizontal motion admitted by these joints is approximately ± 30 deg.

It is noted that conventional aileron control surfaces are omitted from the aircraft's final design. This feature is a direct result of span variations created by the dynamic range of morphing configurations. Therefore, the wrist joints are designed in such a manner that they allow both horizontal sweep and rolling twist. This motion is accomplished by creating a floating joint that closely mimics the

Fig. 2 Different sweep configurations of MAV.

various ranges of motion attainable by an automobile's universal joint.

The wing surface must be kept continuous for any configuration of sweeping because of aerodynamic concerns. This vehicle ensures such continuity by layering featherlike structures within the joint. These structures retract onto each other under the wing when both the inboard and outboard are swept back. Conversely, they create a fanlike cover across the ensuing gap when the inboard is swept back and the outboard is swept forward. The contraction and expansion of the surface area created by these structures is smoothly maintained by means of a tract implemented on the outer regions of each member.

Spars, formed from hollow shafts of carbon fiber, are placed along the leading edge of each wing. These spars act as both a rigid source to maintain the leading-edge curvature and a connection of each independent wing joint. The inboard spar is translated horizontally by a servo-driven linear actuator located inside the fuselage. The inboard spar is then connected to the inboard wing section at the elbow joint located on the outside of the fuselage. The inboard spar then connects at the wrist joint to the outboard spar at roughly the quarter-span point. The outboard wing region is activated independently of the inboard region by means of a servo attached at the wrist. The Reynolds number for this vehicle is of the order of 1.2×10^5.

The resulting vehicle is able to achieve a wide range of sweep configurations. These configurations include different values of sweep for the right wing and left wing along with the inboard section and outboard section; however, this paper will limit the morphing to only symmetric configurations with the inboard section and outboard section having the same sweep such as shown in Fig. 2. Such a reduction is required to reduce the degrees of freedom to a manageable amount and facilitate presentation of the flight dynamics.

B. Modeling

The flight dynamics are analyzed using Athena Vortex Lattice (AVL) to estimate the aerodynamics [37]. This low-order code makes assumptions that the flow is incompressible and inviscid; however, it is widely used in the community and is particularly accurate for analyzing micro air vehicles with thin wings [38–45]. The aerodynamics of the wings are estimated along with flow associated with slender bodies such as the fuselage.

AVL assumes quasi-steady flow so unsteady vorticity shedding is neglected. More precisely, it assumes the limit of small reduced frequency, which means that any oscillatory motion must be slow enough so that the period of oscillation is much longer than the time it takes the flow to traverse an airfoil chord. This assumption is valid for virtually any expected flight maneuver of the vehicle. Also, the rates in roll, pitch, and yaw used in the computations must be slow enough so that the resulting relative flow angles are small as judged by the dimensionless rotation rate parameters.

The introduction of symmetric morphing alters the aerodynamics and associated values of stability derivatives. These variations resulting from morphing the sweep symmetrically are primarily restricted to some derivatives of normal force and all the derivatives of pitch moment. As such, the standard state-space representation of the linearized dynamics is modified in Eq. (26) to reflect the dependency of these derivatives on the morphing trajectory given as $\mu(t)$. Note that the states are defined in terms of perturbations from trim values. The representation of a morphing aircraft having independent shape and flight control, as in a LTV system, has been discussed earlier [16] in the literature

$$\begin{bmatrix} \dot{u} \\ \dot{w} \\ \dot{q} \\ \dot{\theta} \end{bmatrix} = \begin{bmatrix} X_u & X_w & X_q & -g\cos\theta_0 \\ Z_u & Z_w(\mu) & u_0 & -g\sin\theta_0 \\ M_u(\mu) & M_w(\mu) & M_q(\mu) & 0 \\ 0 & 0 & 1 & 0 \end{bmatrix} \begin{bmatrix} u \\ w \\ q \\ \theta \end{bmatrix} \tag{26}$$

We note that in general, all the stability derivatives vary as a function of the morphing trajectory; however, some of them show relatively smaller variation (over the entire morphing range), when compared with others. Accordingly, in Eq. (26), those stability derivatives that do demonstrate substantial variation during morphing are represented as functions of μ, while those that demonstrate relatively smaller variation during morphing, are approximated as constants. The analysis of time-varying dynamics using the poles defined in Eq. (13) requires the state-space system in Eq. (26) to be formulated as a single fourth-order differential equation. In this case, the equation involving the normal velocity w is considered. The equations involving the other states can also be derived; however, the poles associated with the normal velocity are sufficient to characterize the entire system since any pole set associated with a different state is obtained by a transformation of these poles. The general form of the fourth-order expression for normal velocity is given in Eq. (27) by including time-varying coefficients A_0, A_1, A_2, and $A_3 \in \mathcal{R}$, which are lengthy and therefore defined in the Appendix

$$\frac{\mathrm{d}^4 w}{\mathrm{d}t^4} + A_3(t)\frac{\mathrm{d}^3 w}{\mathrm{d}t^3} + A_2(t)\frac{\mathrm{d}^2 w}{\mathrm{d}t^2} + A_1(t)\frac{\mathrm{d}w}{\mathrm{d}t} + A_0(t)w = 0 \tag{27}$$

The coefficients in Eq. (27) have significantly different dependencies on the morphing in that while all of them depend on the stability derivatives of Z_w, M_w, M_q, and M_u, which vary with morphing, not all of them depend on the rate of change of these stability derivatives. For instance, the value of A_0 depends on both the first and second time derivatives for all four of these stability derivatives [see Eq. (A24)]; conversely, A_3 depends only on the first derivative and second time derivatives for M_q and M_u [see Eq. (A1)]. An observation of Eq. (A1) also shows that the effect of morphing on A_3 can even be further mitigated by noting that A_3 depends on the morphing value but not the morphing rate if the morphing trajectory is chosen so as to satisfy $\frac{\dot{M}_u}{\dot{M}_q} = \frac{\ddot{M}_u}{\ddot{M}_q} = -\frac{Z_u}{u_o}$. As such, the time variations of certain stability derivatives only affect certain coefficients depending on the rate of change of the morphing trajectory.

Also, certain morphing trajectories have a potential to cause a bifurcation that reduces the order of the dynamics. As is evident from Eqs. (A1), (A7), (A14), and (A24), the coefficients in Eq. (27) each contain a fraction with the same denominator; and this denominator becomes zero for certain morphing trajectories. The loss of order is equivalently viewed by multiplying Eq. (27) by this denominator so that the dependence on $\frac{\mathrm{d}^4 w}{\mathrm{d}t^4}$ is scaled by zero.

Finally, note that substitution of $A_0(t), A_1(t), A_2(t)$, and $A_3(t)$ from Eqs. (A1), (A7), (A14), and (A24) in Eq. (13), leads to an analytical representation of the characteristic equation of this morphing aircraft. When the aircraft is not morphing, then by substitution of the time derivatives of p_{4i}, Z_w, M_u, M_w, and M_q in Eqs. (13), (A1), (A7), (A14), and (A24) as being identically zero, this characteristic equation does indeed reduce to that of a time-invariant aircraft available in standard textbooks on flight dynamics [46]. Equations (13), (A1), (A7), (A14), and (A24) thus represent a generalization of the standard characteristic equation of a time-invariant aircraft, to a morphing aircraft.

IV. Time-Varying Effects of Morphing

A. State Responses to Disturbances Occurring During Morphing

The flight dynamics of the vehicle shown in Fig. 2 are analyzed during symmetric morphing from a backward sweep to having no sweep. Specifically, the sweep varies from +30 to 0 deg in 1 s and then remains at a sweep angle of 0 deg for each wing. This morphing would be valuable when transitioning from a dive to straight-and-level flight in a manner similar to biological systems like gulls and hawks. This transition, especially when operating immersed in urban environments that are dense in obstacles, may still require rapid maneuvering for positioning along with gust rejection so the flight dynamics during the morphing remain of critical importance.

Figure 3 demonstrates the state responses to disturbances occurring during morphing. Specifically, an impulse disturbance is assumed to strike the aircraft at the same instant when the aircraft just begins morphing. Thus, though the aircraft is flying at trim at $t = 0^-$, it becomes offtrim at $t = 0$ due to the effect of the disturbance. The

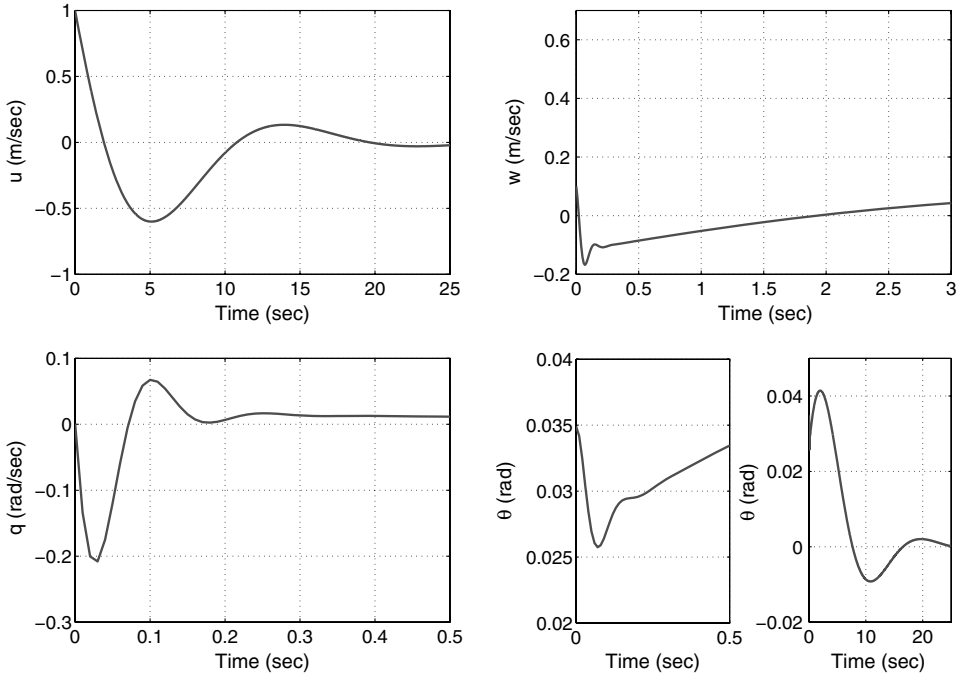

Fig. 3 Longitudinal states during morphing from +30 to 0 deg over 1 s : Forward velocity (upper left), normal velocity (upper right), pitch rate (lower left), pitch attitude (lower center and right).

aircraft is a linear time-varying system for the initial 1 s; however, the response still resembles the traditional modes for a linear time-invariant system. The pitch rate and vertical velocity show a high-frequency response that is heavily damped to resemble the short-period mode; conversely, the airspeed and pitch angle are dominated by a low-frequency response that is lightly damped to resemble a phugoid mode.

B. Time-Varying Poles and Eigenvectors

The time-varying poles associated with Fig. 3 are computed from Eq. (13) and shown in Fig. 4 along with the time-invariant poles that ignore the time-varying effects of morphing. In their computation, the initial conditions on the LTV poles have been chosen so that the solution of Eq. (13) results in bounded poles. These results indicate several characteristics of LTV poles. Observe that the LTI poles associated with the short-period mode remain nearly constant with morphing angle; however, the time-varying poles of $p_{41}(t)$ and $p_{42}(t)$, which are initially closest in value to the LTI short-period poles, decay to a value close to zero at a rate similar to decay of the w and q state responses due to damping. Also, note that the LTV poles $p_{43}(t)$ and $p_{44}(t)$ show the low magnitude and slow decay associated with a phugiod mode. Finally, $p_{41}(t)$ and $p_{43}(t)$ are quite distinct from each other during the initial phase of the morphing; however, toward the end of the morphing segment they are quite close to each other.

The modes $\phi_{4i} = \exp(\int_0^t p_{4i}(t))$ associated with each pole in Fig. 4 are shown in Fig. 5. Since the decomposition of the response depends on the eigenvectors and these modes, they must be considered when evaluating the flight dynamics. Note that though

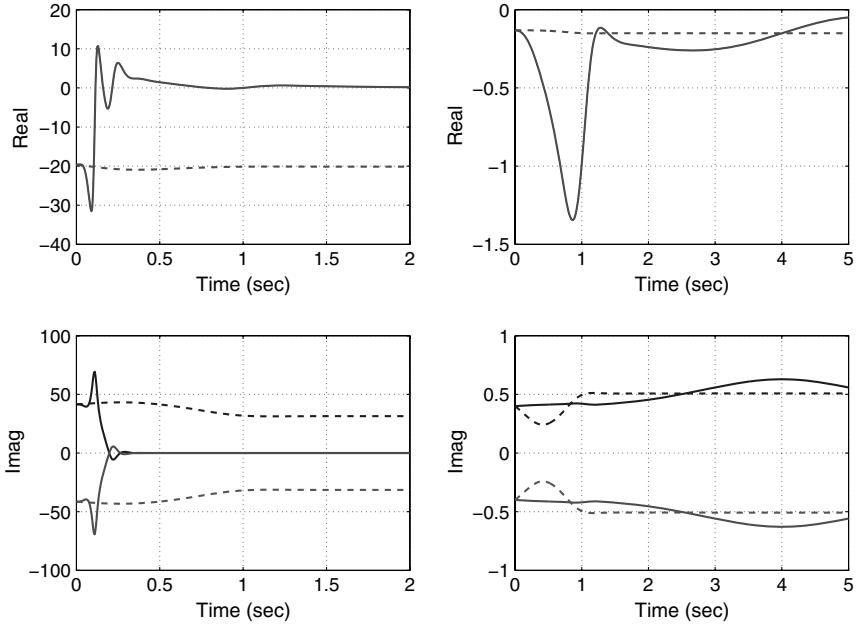

Fig. 4 Linear time-varying poles (—) and linear time-invariant poles (– – –) during morphing from +30 to 0 deg over 1 s : real part (upper left) and imaginary part (lower left) of p_{41} and p_{42}, real part (upper right), and imaginary part (lower right) of p_{43} and p_{44}.

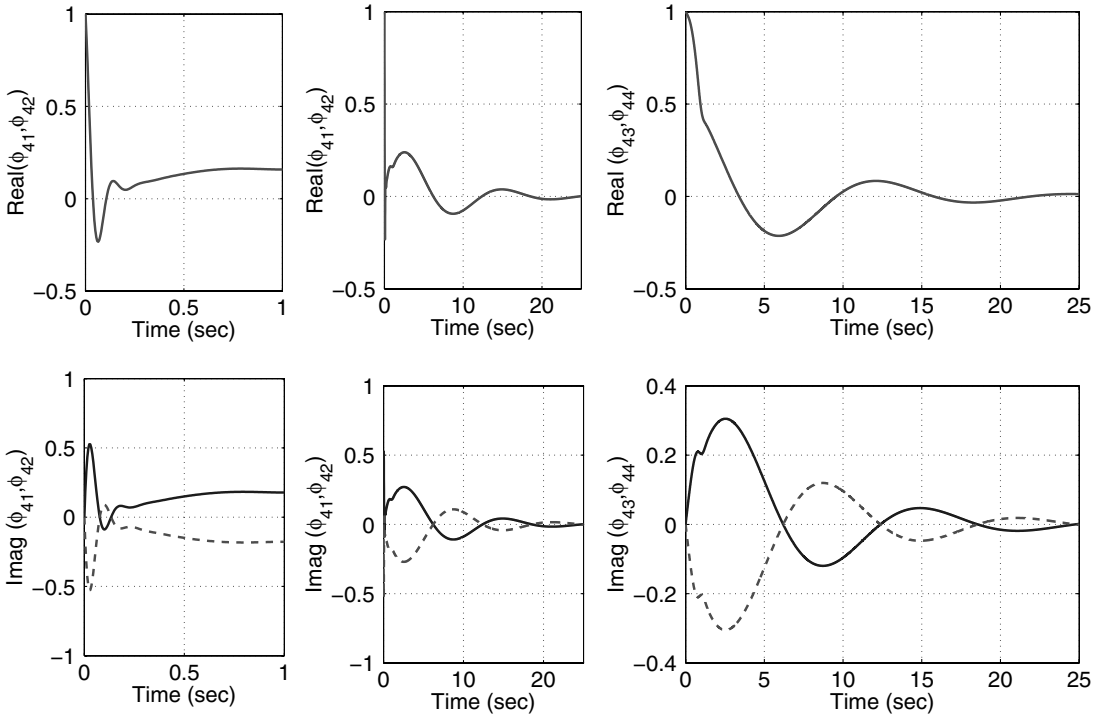

Fig. 5 Modes associated with time-varying poles during morphing from +30 to 0 deg over 1 s: real part (upper left and center) and imaginary part (lower left and center) of ϕ_{41} and ϕ_{42}, real part (upper right) and imaginary part (lower right) of ϕ_{43} and ϕ_{44}.

our primary interest in these modes is only during the morphing segment (which ends at 1 s), yet they are demonstrated in Fig. 5 for longer times for the purpose of evaluating their stability. Toward the end of the morphing segment, $p_{41}(t)$ and $p_{43}(t)$ are nearly indistinct from each other; this is also reflected in the time-varying modes. During the initial part of the morphing segment, the modes $\phi_{41}(t)$ and $\phi_{42}(t)$ show the fast initial variation that is characteristic of a typical short period. However, these modes continue to remain significant even after this initial decay; and during the time-invariant segment, they show variation more consistent with the phugoid mode. The modes $\phi_{43}(t)$ and $\phi_{44}(t)$ show a clear transition around 1 s (which is when the morphing ends), after which their nature is quite consistent with that of a typical time-invariant phugiod mode. Indeed, the real parts of $\phi_{43}(t)$ and $\phi_{44}(t)$ are remarkably similar to the response of forward velocity, which is predominately due to the phugoid mode, in Fig. 3.

The nature of the modes agrees with the mathematical properties that relate them to both the response and the poles. The responses of Fig. 3 are oscillatory and indeed the poles of Fig. 4 are complex conjugates so the modes of Fig. 5 are also complex conjugates. The real and imaginary parts of the modes are noted in Eq. (17) to be 90° out of phase and indeed this phase difference is seen for $\phi_{41}(t)$ and $\phi_{43}(t)$. Also, the state response should be proportional to the real part of the mode as noted in Eq. (17) which is demonstrated by the vertical

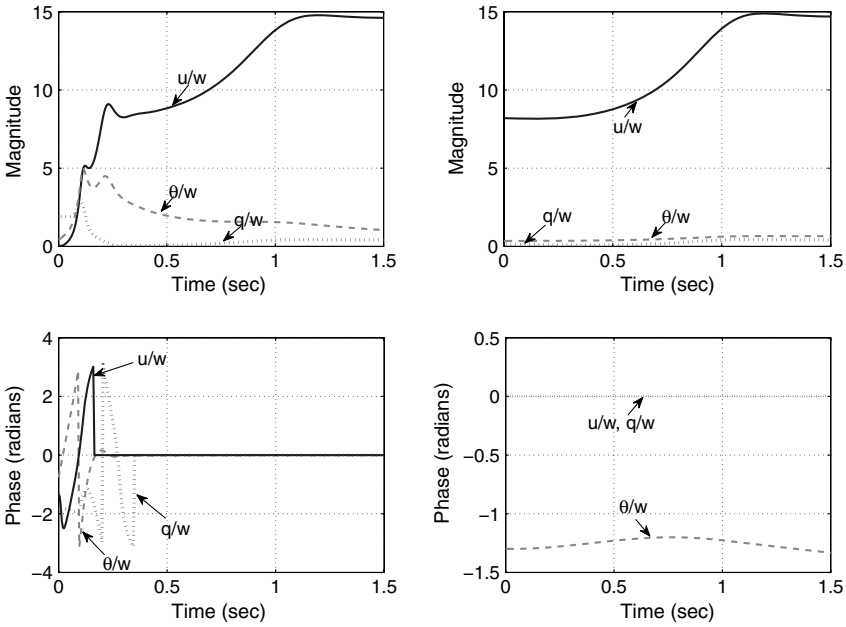

Fig. 6 Normalized eigenvectors associated with time-varying modes during morphing from +30 to 0 deg over 1 s: magnitude (upper left) and phase (lower left) of v_1 and magnitude (upper right) and phase (lower right) of v_3.

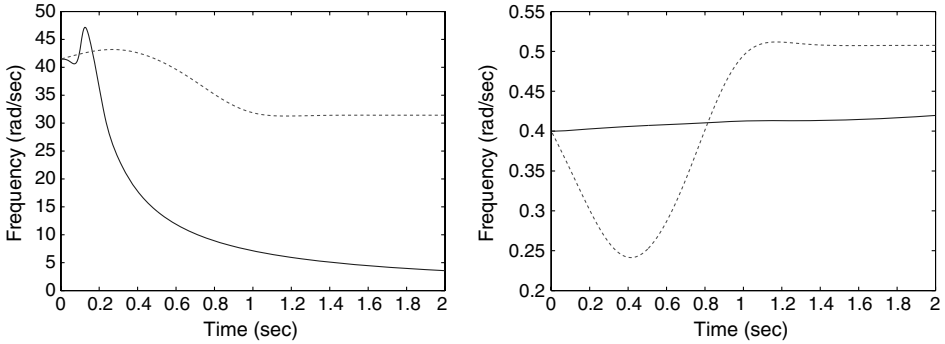

Fig. 7 Natural frequency associated with linear time-varying poles (—) and linear time-invariant poles (– – –) during morphing from +30 to 0 deg over 1 s: poles 1 and 2 (left) and poles 3 and 4 (right).

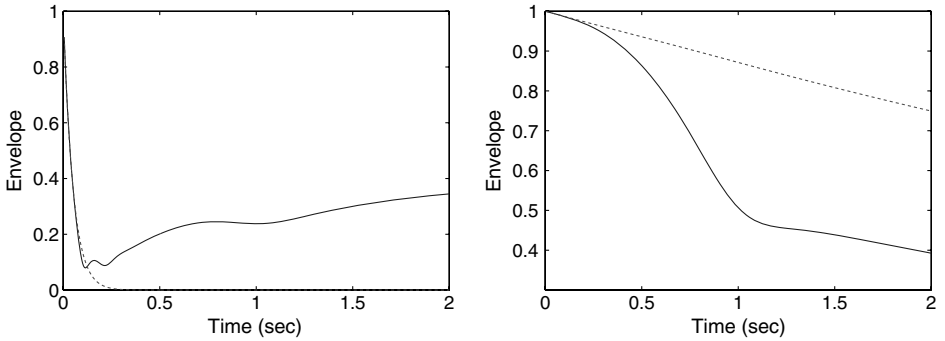

Fig. 8 Envelope associated with linear time-varying poles (—) and linear time-invariant poles (– – –) during morphing from +30 to 0 deg over 1 s: poles 1 and 2 (left) and poles 3 and 4 (right).

velocity in Fig. 3 matching the real part of $\phi_{41}(t)$ (during the morphing segment) and the forward velocity in Fig. 3 matching the real part of $\phi_{43}(t)$.

The issue of stability is directly indicated by the modes of Fig. 5. These modes demonstrate that the system during this morphing trajectory has asymptotic stability since the magnitude of each mode decays to zero as time increases. This result correlates with the responses shown in Fig. 3 that obviously return to equilibrium. Note that one guarantee for asymptotic stability is having negative real part for the time-varying pole. The real part of the poles $p_{43}(t)$ and $p_{44}(t)$ in Fig. 4 are indeed always negative; however, the real part of the poles $p_{41}(t)$ and $p_{42}(t)$ are sometimes positive; so the modes $\phi_{41}(t)$ and $\phi_{42}(t)$ must be computed to ascertain stability.

Finally, the eigenvectors associated with each mode of Fig. 5 are graphed in Fig. 6 to show the relative response of each vehicle state as normalized by the vertical velocity. These eigenvectors, similarly as the poles and modes, show both short-period characteristics and phugoid characteristics. The eigenvector $v_1(t)$ initially shows short-period motion, with little variation in forward velocity and a phase difference of 90° between pitch rate and vertical velocity, after which

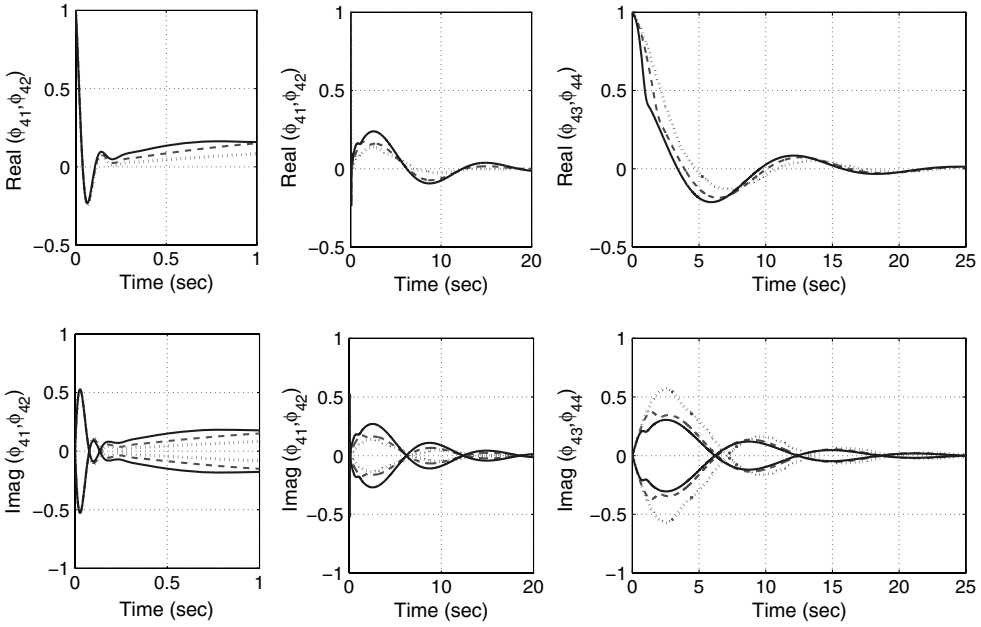

Fig. 9 Modes associated with time-varying poles during morphing from +30 to 0 deg over 1 s (—) and 2 s (– – –) and 4 s (...): real part (upper left and center) and imaginary part (lower left and center) of ϕ_{41} and ϕ_{42}, real part (upper right) and imaginary part (lower right) of ϕ_{43} and ϕ_{44}.

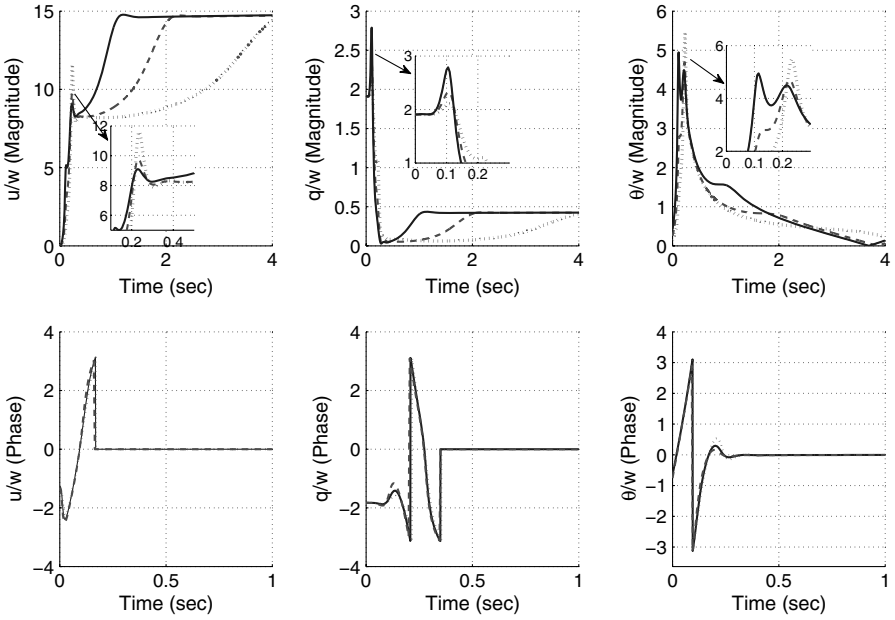

Fig. 10 Normalized eigenvectors of v_1 associated with time-varying modes during morphing from +30 to 0 deg over 1 s (—) and 2 s (– – –) and 4 s (...): magnitude (upper left) and phase (lower left) of forward velocity (u/w), magnitude (upper center) and phase (lower center) of pitch rate (q/w), Magnitude (upper right) and phase (lower right) of pitch angle (θ/w).

the phugoid response is evident. The eigenvector $v_3(t)$ steadily transitions to the phugiod response which is primarily motion in forward velocity and pitch angle which are 90° out of phase. Also, note that these eigenvectors nearly converge to similar magnitudes and phases except for a 90° difference in phase of the pitch angle between $v_1(t)$ and $v_3(t)$.

In summary, the initial times $\phi_{41}(t)$ and $v_1(t)$ show the characteristics of a typical short period; but after the w and q state responses have been significantly damped out, $\phi_{41}(t)$ and $v_1(t)$ transition to show characteristics of a typical phugoid. On the other hand, $\phi_{43}(t)$ and $v_3(t)$ show the characteristics of a typical phugoid for all time. The superposition of $\phi_{41}(t)$, $\phi_{42}(t)$, $\phi_{43}(t)$, $\phi_{44}(t)$, $v_1(t)$, $v_2(t)$, $v_3(t)$, and $v_4(t)$ [in the manner of Eq. (15)] leads to an accurate replication of the state response demonstrated in Fig. 3.

C. Modal Interpretation

A modal interpretation of the poles in Fig. 4 is conducted to relate these mathematical constructs to standard parameters associated with flight dynamics. The parameters associated with the LTI poles are directly computed from the LTI poles themselves while their LTV counterparts are computed by using Eqs. (18) and (19).

The natural frequencies obtained from the time-varying and time-invariant poles have some commonalities but also some clear differences, as shown in Fig. 7. The values are reasonably close for the entire trajectory when considering the poles associated with the phugoid mode; however, the values are only close for a short time when considering the short-period mode. The difference in natural frequencies for the short-period mode results from the relationship of the time-varying poles to the states. Essentially, the short-period pole

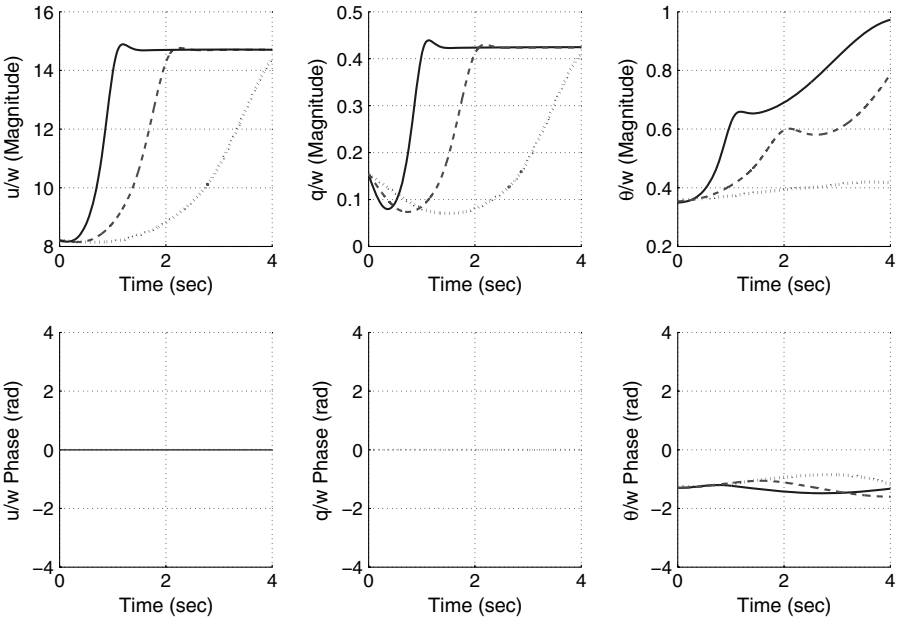

Fig. 11 Normalized eigenvectors of v_3 associated with time-varying modes during morphing from +30 to 0 deg over 1 s (—) and 2 s (– – –) and 4 s (...): magnitude (upper left) and phase (lower left) of forward velocity (u/w), magnitude (upper center) and phase (lower center) of pitch rate (q/w), magnitude (upper right) and phase (lower right) of pitch angle (θ/w).

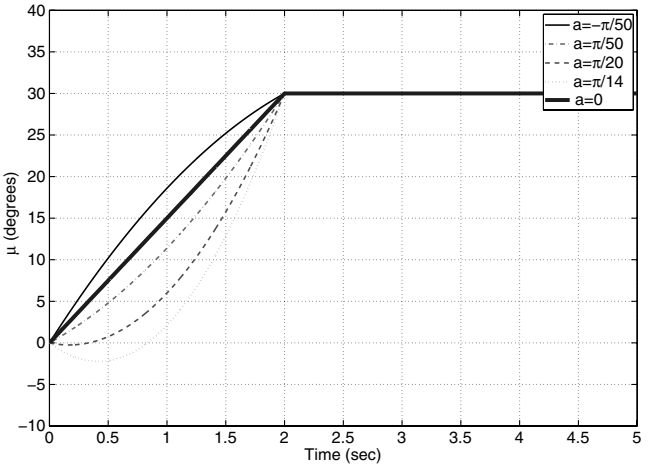

Fig. 12 Morphing trajectories with $a = -\frac{\pi}{50}$ (—), $a = 0$ (—), $a = \frac{\pi}{14}$ (– – –), $a = \frac{\pi}{20}$ (– – –), $a = \frac{\pi}{50}$ (...).

$p_{41}(t)$ is initially relating the oscillatory behavior of the response but the significant decrease in response magnitude due to damping is actually reflected by the time-varying pole decaying to a value close to zero.

The envelope that bounds the responses are shown in Fig. 8. As with the natural frequency, the parameters differ for the time-varying poles and the time-invariant poles. In the case of the envelope corresponding to ϕ_{41}, this envelope initially bounds the response of the pitch rate and vertical velocity which dominate the short-period response but then, after these states have been damped out, the envelope reflects the bound on the pitch angle.

V. Effect of Linear Morphing Trajectories

The relationship between the state responses and the time-varying dynamics is further evidenced by considering different trajectories. In this case, a set of simulations begin with a backward sweep of +30 deg and transition to having no sweep of 0 deg over 1, 2, and 4 s.

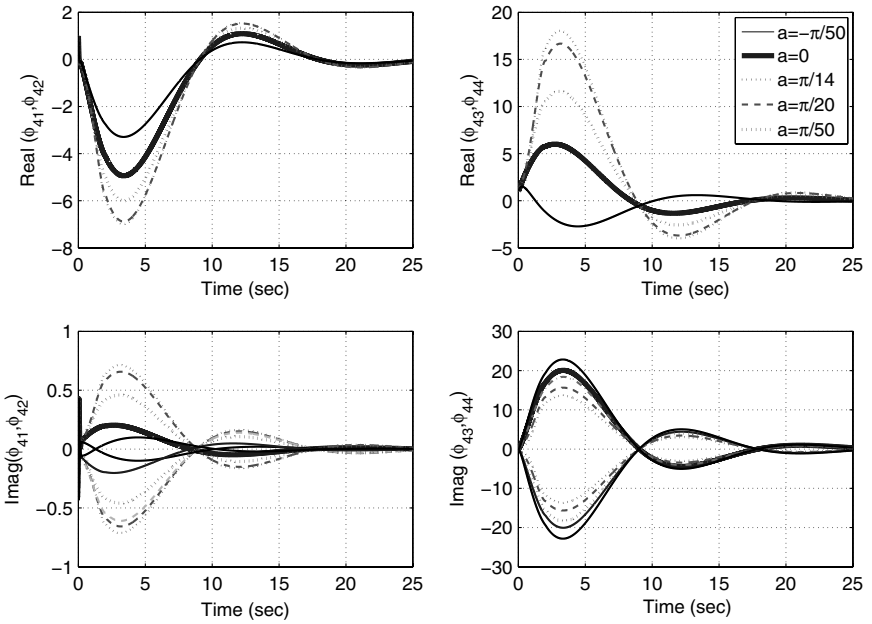

Fig. 13 Time-varying modes during morphing from 0 to 30 deg with $a = -\frac{\pi}{50}$ (—), $a = 0$ (—), $a = \frac{\pi}{14}$ (– – –), $a = \frac{\pi}{20}$ (– – –), $a = \frac{\pi}{50}$ (...).

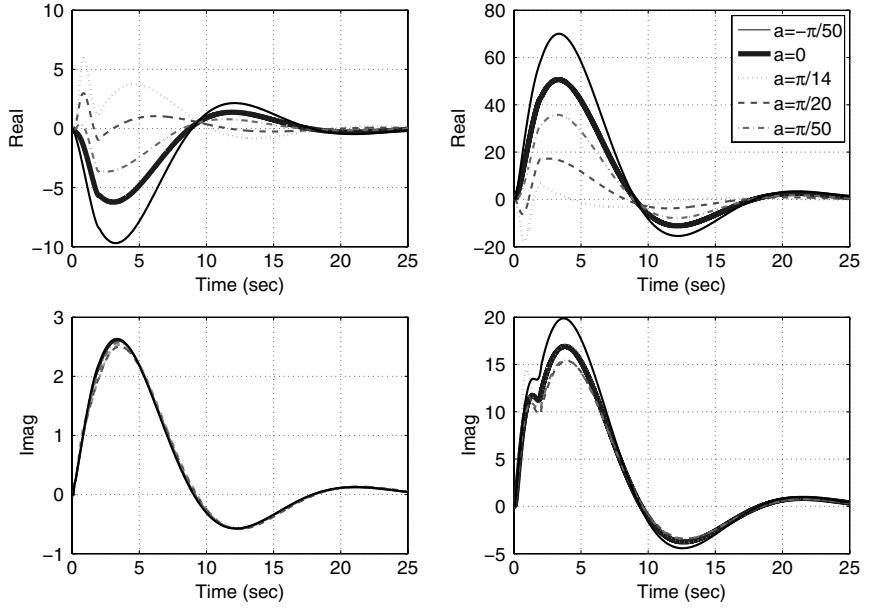

Fig. 14 Sensitivity of time-varying modes during morphing from 0 to 30 deg with $a = -\frac{\pi}{50}$ (—), $a = 0$ (—), $a = \frac{\pi}{14}$ (– – –), $a = \frac{\pi}{20}$ (– – –), $a = \frac{\pi}{50}$ (...).

The modes are computed in Fig. 9 from the time-varying poles associated with these morphing trajectories. The effect of the morphing rate is most evidenced in magnitude variations after 0.2 s. The lack of variation before 0.2 s results from the fact that morphing remains slower than the rapid decay caused by short-period damping. The actual variations are then largest between 0.2 and 4.0 s, which reflects the variations in damping of the phugoid mode (from one morphing trajectory to the next). The sweep is identical for all trajectories after 4.0 s and therefore the modes rapidly converge to similar behavior associated with their respective phugoid mode. Except for this difference in magnitudes, the modes have similar nature for each morphing trajectory in that all remain complex conjugates with similar frequency of oscillation and even guarantee asymptotic stability due to their convergence to the origin.

The eigenvectors of v_1 are given for each morphing trajectory in Fig. 10. It is seen that the influence of the morphing rate on the phase is negligible, while there is a strong influence on the magnitudes. In particular, the peak magnitudes are considerably different: the forward velocity eigenvector shows the largest overshoot for the smallest morphing rate and the smallest overshoot for the largest morphing rate. This trend is reversed for the pitch rate eigenvector, which shows the largest overshoot for the largest morphing rate and the smallest overshoot for the smallest morphing rate. In the case of pitch angle, there are actually two peaks for the largest morphing rate, which merge into a single peak as the morphing rate is decreased. For longer times, the eigenvectors of v_1 begin to transition from resembling a short period to resembling a phugoid.

The effect of morphing rate on $v_3(t)$ [shown in Fig. (11)] is relatively more benign; as such, these eigenvectors show no significant peak overshoots, and both forward velocity and pitch rate reach their steady-state values at the same time as the morphing ends. There is no significant influence of the morphing rate on the phases of $v_3(t)$.

VI. Effect of Quadratic Morphing Trajectories

In this section, the sensitivity of the flight dynamics to quadratic morphing trajectories is evaluated. The sensitivity of the time-varying modes from is computed from Eqs. (23) and (27) and validated by considering the set of morphing trajectories presented in Eq. (28). In particular, a set of six different values of the parameter of a associated with the trajectories in Fig. 12 are evaluated. Note that all these trajectories share the same *average* morphing rate (when averaged over the morphing duration of 2 s), but different *instantaneous* morphing rates

$$\mu(t) = \begin{cases} at + \left(\frac{\pi}{12} - 2a\right)t^2 & 0 \le t \le 2 \\ \frac{\pi}{6} & t \ge 2 \end{cases} \tag{28}$$

The flight dynamics are considerably varied across the set of morphing trajectories. The associated time-varying modes are shown in Fig. 13. These modes share similarity in shape; however, their magnitudes differ dramatically with variations in the instantaneous morphing rate.

The sensitivity as determined using Eq. (24) is presented in Fig. 14. In this case, the real part of the modes are shown to have a relatively high sensitivity, while the imaginary parts have a relatively low sensitivity. The difference in sensitivity of each mode relative to the other is evident both pointwise in time, as well as in the time integral sense.

VII. Conclusions

The flight dynamics of a morphing aircraft must consider the time-varying effects. Toward this end, a variable wing sweep morphing aircraft is represented as a linear time-varying system, which is then studied from a flight dynamics perspective. An analytical representation of the time-varying characteristic equation of the longitudinal dynamics is obtained, and this represents a generalization of the well-known characteristic equation of linear time-invariant aircraft. The concept of a time-varying pole is adopted and the time-varying poles corresponding to the characteristic equation derived in this paper are shown to have clear differences from the corresponding time-invariant counterparts. Further, this time-varying pole is demonstrated to have relevance to standard concepts such as mode frequency and envelope that provide considerable practical insight into the flight dynamics. A continuous sensitivity method is then used to evaluate the sensitivity of the time-varying modes to different morphing trajectories. A tool for properly evaluating the flight dynamics of morphing aircraft with varying morphing trajectories is thus demonstrated.

Appendix

The coefficients of the time-varying characteristic Eq. (27) are presented below, for $\theta_0 \approx 0$. The third derivative of normal velocity $\frac{d^3w}{dt^3}$ in Eq. (27) is scaled by A_3 and defined in Eq. (A1) using Eqs. (A2–A6)

$$A_3(t) = -Z_w(t) - \frac{N_1\dot{M}_u + N_2\dot{M}_q + N_3\ddot{M}_u + N_4\ddot{M}_q + N_5}{D_1\dot{M}_u + D_2\dot{M}_q + D_3} \tag{A1}$$

$$D_1 = -Z_u u_0^2; \qquad D_2 = Z_u^2 u_0 \tag{A2}$$

$$D_3 = Z_u^2(u_0 M_q^2 - gZ_u - X_u u_0 M_q) + u_0^2 M_u(u_0 M_u + X_u Z_u - 2Z_u M_q) \tag{A3}$$

$$N_1 = (2u_0 M_u(t) - 3Z_u M_q(t))u_0^2$$
$$N_2 = (3Z_u M_q(t) - 2u_0 M_u(t))Z_u u_0 \tag{A4}$$

$$N_3 = -Z_u u_0^2; \qquad N_4 = Z_u^2 u_0 \tag{A5}$$

$$N_5 = (X_u + M_q)(-gZ_u^3 + Z_u^2 u_0 M_q(M_q - X_u) + Z_u u_0^2 M_u(X_u - 2M_q) + u_0^3 M_u^2) \tag{A6}$$

The second derivative of normal velocity $\frac{d^2w}{dt^2}$ in Eq. (27) is scaled by A_2 defined in Eq. (A7) using Eqs. (A8–A12)

$$A_2(t) = -3\dot{Z}_w - X_w Z_u - u_0 M_w - \frac{\bar{N}_1\dot{M}_u^2 + \bar{N}_2\dot{M}_u\dot{M}_q + \bar{N}_3(t)\dot{M}_u + \bar{N}_4\dot{M}_q + \bar{N}_5\ddot{M}_u + \bar{N}_6\ddot{M}_q + N_7}{D_1\dot{M}_u + D_2\dot{M}_q + D_3} \tag{A7}$$

$$\bar{N}_1 = -2u_0^3; \qquad \bar{N}_2 = 2Z_u u_0^2 \tag{A8}$$

$$\bar{N}_3 = u_0^2[(X + Z_u Z_w)(2X_u + M_q) - 3(X_u X + u_0 M_u M_q)] - 2u_0(Z_w u_0(X - Z_u M_q) - Z_u(u_0 M_q^2 - gZ_u)) \tag{A9}$$

$$\bar{N}_4 = Z_u u_0[(X_u X + u_0 M_u M_q) - 3M_q(X + Z_u Z_w)] + 2Z_u^2 M_u(X + Z_u Z_w) \tag{A10}$$

$$\bar{N}_5 = u_0^2(X + Z_u Z_w); \qquad \bar{N}_6 = -Z_u u_0(X + Z_u Z_w) \tag{A11}$$

$$\bar{N}_7 = -(X_u Z_w + X_u M_q + Z_w M_q)(-gZ_u^3 + Z_u^2 u_0 M_q(M_q - X_u) + Z_u u_0^2 M_u(X_u - 2M_q) + u_0^3 M_u^2) \tag{A12}$$

$$X = X_u Z_u + u_0 M_u; \qquad Z = u_0 M_q^2 - g Z_u \tag{A13}$$

The first derivative of normal velocity $\frac{\mathrm{d}w}{\mathrm{d}t}$ in Eq. (27) is scaled by A_1 defined in Eq. (A14) using Eqs. (A15–A23)

$$A_1(t) = 3\ddot{Z}_w + X_w X + 2u_0\dot{M}_w + u_0 M_w M_q + \frac{\begin{bmatrix} \tilde{N}_1 \dot{Z}_w \dot{M}_u + \tilde{N}_2 \dot{Z}_w \dot{M}_q + \tilde{N}_3 \dot{Z}_w \ddot{M}_u + \tilde{N}_4 \dot{Z}_w \ddot{M}_q + \tilde{N}_5 \dot{Z}_w + \tilde{N}_6 \dot{M}_u^2 + \tilde{N}_7 \dot{M}_u \dot{M}_q \\ + \tilde{N}_8 \dot{M}_u \ddot{M}_q + \tilde{N}_9 \dot{M}_u + \tilde{N}_{10} \dot{M}_q^2 + \tilde{N}_{11} \dot{M}_q \ddot{M}_u + \tilde{N}_{12} \dot{M}_q + \tilde{N}_{13} \ddot{M}_u + \tilde{N}_{14} \ddot{M}_q + \tilde{N}_{15} \end{bmatrix}}{D_1 \dot{M}_u + D_2 \dot{M}_q + D_3} \tag{A14}$$

$$\tilde{N}_1 = 2u_0^2(3Z_u M_q - 2u_0 M_u); \qquad \tilde{N}_2 = Z_u u_0(4u_0 M_u - 6Z_u M_q)$$
$$\tilde{N}_3 = 2Z_u u_0^2; \tilde{N}_4 = -2Z_u^2 u_0 \tag{A15}$$

$$\tilde{N}_5 = -2Z_u^2(-gX + M_q(u_0 M_q^2 - gZ_u)) - 2u_0(X_u X + u_0 M_u M_q)(X - Z_u M_q + Z_u(X_u(X_u X + u_0 M_u M_q) + M_u(u_0 M_q^2 - gZ_u))) \tag{A16}$$

$$\tilde{N}_6 = 2u_0^3(Z_w + M_q); \qquad \tilde{N}_7 = -2u_0^2(u_0 M_u + Z_u(Z_w + M_q))$$
$$\tilde{N}_8 = -Z_u u_0^2 \tag{A17}$$

$$\tilde{N}_9 = u_0^2(X_u X + u_0 M_u M_q)(Z_w + M_q) - Z_u u_0(-gX + M_q Z) + u_0(2X_u + M_q)(Z_u Z - Z_w u_0 X + Z_u u_0(X_w Z_u + u_0 M_w) - u_0 M_q X) - 2u_0(ZX + u_0(X - Z_u M_q)(X_w Z_u + u_0 M_w)) + 2u_0(Z_w(u_0(X_u X + u_0 M_u M_q) - Z_u Z) + u_0 M_q(X_u X + u_0 M_u M_q)) \tag{A18}$$

$$\tilde{N}_{10} = 2Z_u u_0^2 M_u; \qquad \tilde{N}_{11} = Z_u u_0^2$$

$$\tilde{N}_{12} = -u_0(X + Z_u Z_w)(X_u X + u_0 M_u M_q) + u_0 Z_u(X_u(X_u X + u_0 M_u M_q) + M_u Z) + u_0 3M_q(X^2 - Z_u(X_u X + u_0 M_u M_q) - Z_u^2(X_w Z_u + u_0 M_w) + Z_u Z_w X) + u_0 2M_u(Z_u Z - Z_w u_0 X + Z_u u_0(X_w Z_u + u_0 M_w) - u_0 M_q X) \tag{A20}$$

$$\tilde{N}_{13} = u_0(Z_u(u_0 M_q^2 - gZ_u) - Z_w u_0 X + Z_u u_0(X_w Z_u + u_0 M_w) - u_0 M_q X) \tag{A21}$$

$$\tilde{N}_{14} = u_0(X^2 - Z_u(X_u X + u_0 M_u M_q) - Z_u^2(X_w Z_u + u_0 M_w) + Z_u Z_w X) \tag{A22}$$

$$\tilde{N}_{15} = -(X_w Z_u(X_u + M_q) + gM_u - X_u Z_w M_q + u_0 M_w(X_u + M_q))(-gZ_u^3 + Z_u^2 u_0 M_q(M_q - X_u) + Z_u u_0^2 M_u(X_u - 2M_q) + u_0^3 M_u^2) \tag{A23}$$

The normal velocity w in Eq. (27) is scaled by A_0 defined in Eq. (A24) using Eqs. (A25–A41)

$$A_0(t) = \frac{\mathrm{d}^3 Z_w}{\mathrm{d}t^3} + u_0\dddot{M}_w + X_w(u_0\ddot{M}_u + X_u\dot{X} + u_0 M_u M_q) + M_w(u_0 M_q^2 - gZ_u + u_0\ddot{M}_q) + X_w u_0\ddot{M}_u + u_0 M_w\ddot{M}_q + u_0 M_q\ddot{M}_w + \frac{\begin{bmatrix} \hat{N}_1 \dot{Z}_w \dot{M}_u^2 + \hat{N}_2 \dot{Z}_w \dot{M}_u \dot{M}_q + \hat{N}_3 \dot{Z}_w \dot{M}_u + \hat{N}_4 \dot{Z}_w \dot{M}_q + \hat{N}_5 \dot{Z}_w \ddot{M}_u + \hat{N}_6 \dot{Z}_w \ddot{M}_q \\ + \hat{N}_7 \dot{Z}_w + \hat{N}_8 \dot{M}_u^2 + \hat{N}_9 \dot{M}_u \dot{M}_w + \hat{N}_{10} \dot{M}_u \dot{M}_q + \hat{N}_{11} \dot{M}_u \ddot{Z}_w + \hat{N}_{12} \dot{M}_u \ddot{M}_q \\ + \hat{N}_{13} \dot{M}_u + \hat{N}_{14} \dot{M}_w \dot{M}_q + \hat{N}_{15} \dot{M}_w \ddot{M}_u + \hat{N}_{16} \dot{M}_w \ddot{M}_q + \hat{N}_{17} \dot{M}_w + \hat{N}_{18} \dot{M}_q^2 \\ + \hat{N}_{19} \dot{M}_q \ddot{Z}_w + \hat{N}_{20} \dot{M}_q \ddot{M}_u + \hat{N}_{21} \dot{M}_q + \hat{N}_{22} \ddot{Z}_w \ddot{M}_u + \hat{N}_{23} \ddot{Z}_w \ddot{M}_q + \hat{N}_{24} \ddot{Z}_w \\ + \hat{N}_{25} \ddot{M}_u + \hat{N}_{26} \ddot{M}_q + \hat{N}_{27} \end{bmatrix}}{D_1 \dot{M}_u + D_2 \dot{M}_q + D_3} \tag{A24}$$

$$\hat{N}_1 = 2u_0^3; \qquad \hat{N}_2 = -2Z_u u_0^2 \tag{A25}$$

$$\hat{N}_3 = u_0^2(X_u X + u_0 M_u M_q) + 2u_0(u_0(X_u X + u_0 M_u M_q) - Z_u(u_0 M_q^2 - gZ_u)) - u_0^2 X(2X_u + M_q) \tag{A26}$$

$$\hat{N}_4 = u_0(3Z_u M_q X - Z_u(X_u X + u_0 M_u M_q) - 2u_0 M_u X); \qquad \hat{N}_5 = -u_0^2 X; \qquad \hat{N}_6 = Z_u u_0 X \tag{A27}$$

$$\hat{N}_7 = (u_0(X_u X + u_0 M_u M_q) - Z_u(u_0 M_q^2 - g Z_u))(X_u X + u_0 M_u M_q) - u_0(X_u(X_u X + u_0 M_u M_q) + M_u(u_0 M_q^2 - g Z_u))X + Z_u(-gX + M_q(u_0 M_q^2 - g Z_u))X \tag{A28}$$

$$\hat{N}_8 = 2u_0^3((X_w Z_u + u_0 M_w) - Z_w M_q); \quad \hat{N}_9 = u_0^3(-2u_0 M_u + 3Z_u M_q) \tag{A29}$$

$$\hat{N}_{10} = 2u_0^2(Z_w X - Z_u(X_w Z_u + u_0 M_w)) - Z_u Z_w u_0^2(2X_u + M_q) + 3Z_u Z_w u_0^2 M_q \tag{A30}$$

$$\hat{N}_{11} = u_0^2(-2u_0 M_u + 3Z_u M_q); \qquad \hat{N}_{12} = Z_u Z_w u_0^2 \tag{A31}$$

$$\hat{N}_{13} = -(2X_u u_0 + u_0 M_q)(Z_w(Z_u(u_0 M_q^2 - g Z_u) - u_0 M_q X) + u_0 X(X_w Z_u + u_0 M_w) - Z_u u_0(X_w X + u_0 M_w M_q)) + (u_0^2(X_w Z_u + u_0 M_w) - Z_w u_0^2 M_q)(X_u X + u_0 M_u M_q) + 2u_0((u_0(X_u X + u_0 M_u M_q) - Z_u(u_0 M_q^2 - g Z_u))(X_w Z_u + u_0 M_w) + Z_w((u_0 M_q^2 - g Z_u)X - u_0 M_q(X_u X + u_0 M_u M_q)) - (X_w X + u_0 M_w M_q)(u_0 X - Z_u u_0 M_q)) + Z_u Z_w u_0(-gX + M_q(u_0 M_q^2 - g Z_u)) \tag{A32}$$

$$\hat{N}_{14} = 2Z_u u_0^3 M_u - 3Z_u^2 u_0^2 M_q; \qquad \hat{N}_{15} = Z_u u_0^3; \quad \hat{N}_{16} = -Z_u^2 u_0^2 \tag{A33}$$

$$\hat{N}_{17} = (-Z_u^2 u_0(-gX + M_q(u_0 M_q^2 - g Z_u)) - u_0(X_u X + u_0 M_u M_q)(u_0 X - Z_u u_0 M_q) + Z_u u_0^2(X_u(X_u X + u_0 M_u M_q) + M_u(u_0 M_q^2 - g Z_u))) \tag{A34}$$

$$\hat{N}_{18} = -2Z_u Z_w u_0^2 M_u; \qquad \hat{N}_{19} = (2Z_u u_0^2 M_u - 3Z_u^2 u_0 M_q); \quad \hat{N}_{20} = -Z_u Z_w u_0^2 \tag{A35}$$

$$\hat{N}_{21} = (X_u X + u_0 M_u M_q)(Z_w u_0 X - Z_u u_0(X_w Z_u + u_0 M_w)) - 3u_0 M_q(Z_w(X^2 - Z_u(X_u X + u_0 M_u M_q)) + Z_u^2(X_w X + u_0 M_w M_q) - Z_u X(X_w Z_u + u_0 M_w)) - 2u_0 M_u(Z_w(Z_u(u_0 M_q^2 - g Z_u) - u_0 M_q X) + u_0 X(X_w Z_u + u_0 M_w) - Z_u u_0(X_w X + u_0 M_w M_q)) - Z_u Z_w u_0(X_u(X_u X + u_0 M_u M_q) + M_u(u_0 M_q^2 - g Z_u)) \tag{A36}$$

$$\hat{N}_{22} = Z_u u_0^2; \qquad \hat{N}_{23} = -Z_u^2 u_0 \tag{A37}$$

$$\hat{N}_{24} = -Z_u^2(-gX + M_q(u_0 M_q^2 - g Z_u)) - (X_u X + u_0 M_u M_q)(u_0 X - Z_u u_0 M_q) + Z_u u_0(X_u(X_u X + u_0 M_u M_q) + M_u(u_0 M_q^2 - g Z_u)) \tag{A38}$$

$$\hat{N}_{25} = -u_0(Z_w(Z_u(u_0 M_q^2 - g Z_u) - u_0 M_q X) + u_0 X(X_w Z_u + u_0 M_w) - Z_u u_0(X_w X + u_0 M_w M_q)) \tag{A39}$$

$$\hat{N}_{26} = -u_0(Z_w(X^2 - Z_u(X_u X + u_0 M_u M_q)) + Z_u^2(X_w X + u_0 M_w M_q) - Z_u X(X_w Z_u + u_0 M_w)) \tag{A40}$$

$$\hat{N}_{27} = -(X_w Z_u X_u^2 + X_w u_0 M_u(X_u + M_q) + u_0 M_w M_q^2 - g Z_w M_u)(-gZ_u^3 + Z_u^2 u_0 M_q(M_q - X_u) + Z_u u_0^2 M_u(X_u - 2M_q) + u_0^3 M_u^2) \tag{A41}$$

References

[1] Bowman, J., "Affordability Comparison of Current and Adaptive and Multifunctional Air Vehicle Systems," AIAA Paper 2003-1713, 2003.

[2] Gano, S. E., and Renaud, J. E., "Optimized Unmanned Aerial Vehicle with Wing Morphing for Extended Range and Endurance," AIAA Paper 2002-5668, 2002.

[3] Bowman, J., Sanders, B., and Weisshar, T., "Evaluating the Impact of Morphing Technologies on Aircraft Performance," AIAA Paper 2002-1631, 2002.

[4] Prock, B. C., Weisshaar, T. A., and Crossley, W. A., "Morphing Airfoil Shape Change Optimization with Minimum Actuator Energy as an Objective," AIAA Paper 2002-5401, 2002.

[5] Rusnell, M. T., Gano, S. E., Perez, V. M., Renaud, J. E., and Batill, S. M., "Morphing UAV Pareto Curve Shift for Enhanced Performance," AIAA Paper 2004-1882, 2004.

[6] Secanell, M., Suleman, A., and Gamboa, P., "Design of a Morphing Airfoil for a Light Unmanned Aerial Vehicle using High-Fidelity Aerodynamic Shape Optimization," AIAA Paper 2005-1891, 2005.

[7] Bilgen, O., Kochersberger, K. B., Inman, D. J., and Ohanian, O. J., III, "Novel, Bidirectional, Variable Camber Airfoil via Macro-Fiber Composite Actuators," *Journal of Aircraft*, Vol. 47, No. 1, Jan. 2010, pp. 303–314. doi:10.2514/1.45452

[8] Joshi, S. P., Tidwell, Z., Crossley, W. A., and Ramakrishnan, S., "Comparison of Morphing Wing Strategies Based Upon Aircraft Performance Impacts," AIAA Paper 2004-1722, 2004.

[9] Bae, J., Seigler, T. M., Inman, D. J., and Lee, I., "Aerodynamic and Aeroelastic Considerations of a Variable-Span Morphing Wing," *Journal of Aircraft*, Vol. 42, No. 2, March–April 2005, pp. 528–534. doi:10.2514/1.4397

[10] Gern, F. H., Inman, D. J., and Kapania, R. K., "Structural and Aeroelastic Modeling of General Planform Wings with Morphing Airfoils," *AIAA Journal*, Vol. 40, No. 4, April 2002, pp. 628–637. doi:10.2514/2.1719

[11] Khot, N. S., Eastep, F. E., and Kolonay, R. M., "Method for Enhancement of the Rolling Maneuver of a Flexible Wing," *Journal of Aircraft*, Vol. 34, No. 5, Sept.–Oct. 1997, pp. 673–678. doi:10.2514/2.2228

[12] Love, M. H., Zink, P. S., Stroud, R. L., Bye, D. R., and Chase, C., "Impact of Actuation Concepts on Morphing Aircraft Structures," AIAA Paper 2004-1724, 2004.

[13] Lampton, A., Nicksch, A., and Valasek, J., "Reinforcement Learning of a Morphing-Airfoil Policy and Discrete Learning Analysis," *Journal of Aerospace Computing, Information, and Communication*, Vol. 7, No. 8, Aug. 2010, pp. 241–260.

[14] Obradovic, B., and Subbarao, K., "Modeling and Simulation to Study Flight Dynamics of a Morphable Wing Aircraft," *AIAA Modeling and Simulation Technologies Conference*, AIAA Paper 2009-6240, 2009.

[15] Wickenheiser, A., and Garcia, E., "Optimization of Perching Maneuvers through Vehicle Morphing," *Journal of Guidance, Control, and Dynamics*, Vol. 31, No. 4, July–Aug. 2008, pp. 815–823. doi:10.2514/1.33819

[16] Seigler, T. M., Neal, D. A., Bae, J-S., and Inman, D. J., "Modeling and Flight Control of Large-Scale Morphing Aircraft," *Journal of Aircraft*, Vol. 44, No. 4, July–Aug. 2007, pp. 1077–1087. doi:10.2514/1.21439

[17] Kwak, S., and Yedavalli, R., "New Modeling and Control Design Techniques for Smart Deformable Aircraft Structures," *Journal of Guidance, Control, and Dynamics*, Vol. 24, No. 4, July–Aug. 2001, pp. 805–815. doi:10.2514/2.4782

[18] Johnston, C. O., Neal, D. A., Wiggins, L. D., Robertshaw, H. H., Mason, W. H., and Inman, D. J., "A Model to Compare the Flight Control Energy Requirements of Morphing and Conventionally Actuated Wings," *AIAA Structures, Structural Dynamics and Materials*

Conference, AIAA Paper 2003-1716, 2003.
[19] Cesnik, C. S., Arbor, A., and Brown, E. L., "Active Warping Control of a Joined-Wing/Tail Airplane Configuration," *AIAA Structures, Structural Dynamics and Materials Conference*, AIAA Paper 2003-1715, 2003.
[20] Sanders, B., Eastep, F. E., and Forster, E., "Aerodynamic and Aeroelastic Characteristics of Wings with Conformal Control Surfaces for Morphing Aircraft," *Journal of Aircraft*, Vol. 40, No. 1, Jan.–Feb. 2003, pp. 94–99.
doi:10.2514/2.3062
[21] Sanders, B., Reich, G., Joo, J., and Eastep, F. E., "Air Vehicle Control Using Multiple Control Surfaces," *AIAA Structures, Structural Dynamics and Materials Conference*, AIAA Paper 2004-1887, April 2004.
[22] Tao, G., Chen, S., Fei, J., and Joshi, S. M., "An Adaptive Actuator Failure Comprensation Scheme for Controlling a Morphing Aircraft Model," *IEEE Conference on Decision and Control*, IEEE Publications, Piscataway, NJ, Dec. 2003, pp. 4926–4931.
[23] Spenny, C. H., and Williams, T. E., "Librational Instability of Rigid Space Station due to Translation of Internal Mass," *Journal of Guidance, Control, and Dynamics*, Vol. 14, No. 1, Jan.–Feb. 1991, pp. 31–35.
doi:10.2514/3.20601
[24] Wie, B., "Solar Sail Attitude Control and Dynamics, Part 2," *Journal of Guidance, Control, and Dynamics*, Vol. 27, No. 4, July–Aug. 2004, pp. 536–544.
doi:10.2514/1.11133
[25] Natarajan, A., and Schaub, H., "Linear Dynamics and Stability Analysis of a Two-Craft Coulomb Tether Formation," *Journal of Guidance, Control, and Dynamics*, Vol. 29, No. 4, July–Aug. 2006, pp. 831–838.
doi:10.2514/1.16480
[26] Oliver, R. I., and Asokanthan, S. F., "Control/Structure Integrated Design for Flexible Spacecraft Undergoing On-Orbit Maneuvers," *Journal of Guidance, Control, and Dynamics*, Vol. 20, No. 2, March–April 1997, pp. 313–319.
doi:10.2514/2.4039
[27] Thurman, S. W., and Flashner, H., "Robust Digital Autopilot Design for Spacecraft Equipped with Pulse-Operated Thrusters," *Journal of Guidance, Control, and Dynamics*, Vol. 19, No. 5, Sept.–Oct. 1996, pp. 1047–1055.
doi:10.2514/3.21744
[28] Hill, D. E., Baumgarten, J. R., and Miller, J. T., "Dynamic Simulation of Spin-Stabilized Spacecraft with Sloshing Fluid Stores," *Journal of Guidance, Control, and Dynamics*, Vol. 11, No. 6, Nov.–Dec. 1988, pp. 597–599.
doi:10.2514/3.20360
[29] Venkataraman, S., and Dogan, A., "Dynamic Effects of Trailing Vortex with Turbulence and Time-Varying Inertia in Aerial Refuelling," AIAA Paper 2004-4945, 2004.
[30] Vest, M. S., and Katz, J., "Aerodynamic Study of a Flapping-Wing Micro UAV," AIAA Paper 99-0994, 1999.
[31] Grant, D. T., Abdulrahim, M., and Lind, R., "Flight Dynamics of a Morphing Aircraft Utilizing Independent Multiple-Joint Wing Sweep," AIAA Paper 2006-6505, 2006.
[32] Kamen, E. W., "The Poles and Zeros of a Linear Time Varying System," *Linear Algebra and its Applications*, 1988, Vol. , No. , pp. 263–289, .
[33] O'Brien, R. T., Jr., and Iglesias, P. A., "On the Poles and Zeros of Linear, Time-Varying Systems," *IEEE Transactions on Circuits and Systems-I: Fundamental Theory and Applications*, Vol. 48, No. 5, May 2001, pp. 565–577.
doi:10.1109/81.922459
[34] Zhu, J., and Johnson, C. D., "Unified Canonical Form for Matrices over a Differential Ring," *Linear Algebra and Its Applications*, Vol. 147, No. 1, 1991, pp. 201–248.
doi:10.1016/0024-3795(91)90235-O
[35] Wu, M. Y., "A New Concept of Eigenvalues and Eigenvectors and its Applications," *IEEE Transactions on Automatic Control*, Vol. AC-25, No. 4, 1980, pp. 824–826.
[36] Chakravarthy, A., Grant, D. T., and Lind, R., "Time-Varying Dynamics of a Micro Air Vehicle with Variable-Sweep Morphing," AIAA Paper 2009-6304-853, 2009.
[37] Drela, M., and Youngren, H., "AVL: Aerodynamic Analysis, Trim Calculation, Dynamic Stability Analysis, Aircraft Configuration Development," *Athena Vortex Lattice v3.15*, http://web.mit.edu/drela/Public/web/avl/ [retrieved Dec. 2011].
[38] Stanford, B., Abdulrahim, M., Lind, R., and Ifju, P., "Investigation of Membrane Actuation for Roll Control of a Micro Air Vehicle," *Journal of Aircraft*, Vol. 44, No. 3, May–June 2007, pp. 741–749.
doi:10.2514/1.25356
[39] Traub, L. W., "Experimental Investigation of Annular Wing Aerodynamics," *Journal of Aircraft*, Vol. 46, No. 3, May–June 2009, pp. 988–996.
doi:10.2514/1.39822
[40] Gopalarathnam, A., and Norris, R. K., "Ideal Lift Distributions and Flap Angles for Adaptive Wings," *Journal of Aircraft*, Vol. 46, No. 2, March–April 2009, pp. 562–571.
doi:10.2514/1.38713
[41] Cox, C., Gopalarathnam, A., and Hall, C. E., "Development of Stable Automated Cruise Flap for an Aircraft with Adaptive Wing," *Journal of Aircraft*, Vol. 46, No. 1, Jan.–Feb. 2009, pp. 301–311.
doi:10.2514/1.38684
[42] Boschetti, P., Cardena, E., Amerio, A., and Arevalo, A., "Stability and Performance of a Light Unmanned Airplane in Ground Effect," *AIAA Aerospace Sciences Meeting*, AIAA Paper 2010-293, 2010.
[43] Leong, H. I., Jager, R., Keshmiri, S., and Colgren, R., "Development of a Pilot Training Platform for UAVs using a 6 DOF Nonlinear Model with Flight Test Validation," AIAA Paper 2008-6368, 2008.
[44] Royer, D. A., Keshmiri, S., Sweeten, B. C., and Jones, V., "Modeling and Sensitivity Analysis of the Meridian Unmanned Aircraft," *AIAA Infotech@Aerospace*, AIAA Paper 2010-3468, 2010.
[45] Stewart, K., Blackburn, K., Wagener, J., Czabaranek, J., and Abate, G., "Development and Initial Flight Tests of a Single-Jointed Articulated-Wing Micro Air Vehicle," AIAA Paper 2008-6708, 2008.
[46] Nelson, R. C., *Flight Stability and Automatic Control*, McGraw–Hill, New York, pp. 97–98.